Processing effects during rotating membrane emulsification

CrossMark

David M. Lloyd*, Ian T. Norton, Fotis Spyropoulos

Centre for Formulation Engineering, School of Chemical Engineering, University of Birmingham, Edgbaston, Birmingham B15 2TT, UK

ARTICLE INFO

ABSTRACT

In this study, a rotating membrane emulsification setup incorporating a 6.1 μm pore diameter SPG membrane was used to produce O/W emulsions of average droplet sizes between 23.4 and 216.6 μm. All emulsions consisted of 10 vol% of sunflower oil or silicone oil stabilised by 1 wt% Tween 20. The transmembrane pressure (0.1–1.8 bar), rotational speeds (100–2000 RPM) annular gap width (5–45 mm), dispersed and continuous phase viscosity were all investigated as to their effect on emulsion droplet size and dispersed phase flux. Modification of the dispersed phase flow properties alters the droplet size with four regions being suggested; a decrease in size (as droplet coalescence is minimised), a plateau (size-stable zone), a gradual increase in size (due to transfer of mass via droplet neck) and then a rapid increase (due to jetting). The importance of Taylor vortices development was seen with larger droplets formed in their absence; typically at low rotational speeds, narrow vessel diameters and more viscous continuous phases. It was concluded that the flow behaviour of each phase requires careful consideration to understand the likely formation mechanism(s) during operation. Across the pressure and viscosity ranges investigated, the dispersed phase flux ranged between 50 and 12,500 $\mathrm{Lm^{-2}\,h^{-1}}$ and pore activity was within the range of 0.5–2.7%.

1. Introduction

Emulsions are defined as dispersed systems of at least two immiscible liquid phases, typically an organic and an aqueous phase. One of these phases is dispersed in the form of droplets within a continuous 'bulk' phase. Such systems are encompassed within many food, cosmetic, agrochemical and pharmaceutical formulations and therefore there is great interest in the control of their microstructure. Industrially, emulsions are manufactured using well established processes such as high pressure homogenisers and rotor-stator mixers in which the two phases or pre-emulsion are subjected to high shear forces in the region of 20,000–100,000 $\mathrm{s^{-1}}$ [1]. Droplets are broken down into smaller droplets within turbulent eddies – a phenomenon which is not homogeneous throughout the multi-phase system or over the processing time. As a consequence, the droplet size and size distribution of the resultant emulsion can vary significantly with each batch, which in turn may potentially have an adverse effect on desired functional properties related to structure, as well as stability. Furthermore, these processes require high amounts of mechanical energy which is delivered inefficiently to the system. The rate by which the interface is created far exceeds the rate of which the stabilising molecules (known as surfactants) can adsorb

at the newly created interfaces hence formed droplets can quickly coalesce through a 'back-reaction' that increases emulsion droplet size. This is obviously counter-productive if the intention is to reduce droplet size to a desired value as the energy required to increase interfacial area is essentially wasted. The emulsion may also experience significant thermal stresses within areas of high localised energy dissipation. Ingredients or microstructures which could be susceptible to damage due to high shear and thermal stresses are therefore unsuitable for processing using these conventional emulsification techniques. The disadvantages associated with such processes eliminate to an extent the use of many proteins and starches within formulations, as well as hinder production of specifically designed microstructures such as double emulsions.

However, there is a different approach to emulsification where droplets are created individually and then dispersed into the continuous phase over time. One such method is membrane emulsification. Since its introduction as a novel process to formulate emulsions by Nakashima in the early 1990s [2], membrane emulsification has been a subject of increasing interest to researchers due to the numerous potential advantages it offers [3,4]. The energy input to produce a specific volume of emulsion of identical droplet size is of at least two orders of magnitude lower when compared to traditional formulation processes [5]. With a more gradual increase in interfacial area, formulations no longer require heavy loading of surfactant to stabilise small droplets [6]. The shear forces required to produce droplets are also much lower

* Corresponding author. Tel.: +44 121 414 5260.
  E-mail address: DML066@bham.ac.uk (D.M. Lloyd).

since they are intended to detach rather than break up forming droplets. Membrane emulsification is therefore a more environmentally sustainable process for producing emulsions. Such benefits also offer greater compatibility with fragile ingredients and microstructures (e.g. double emulsions, nano-emulsions) lending itself towards formulating 'smarter' products in future.

At the most fundamental level, the process entails passing dispersed phase through the pores of a membrane into the continuous phase. This is commonly achieved via the application of pressure. Droplets detach from the membrane surface through the generation of a shear force. However, the method by which shear is applied to the system has led to the development of a subset of membrane emulsification processes. The most widely used membrane emulsification process is that of cross-flow membrane emulsification, in which the continuous phase is re-circulated (through a pump) to flow parallel and across the surface of the membrane. Alternatively, the process of dead end membrane emulsification can be used which relies on spontaneous detachment of droplets and therefore no applied shear at all. More recently, rotating membrane emulsification has emerged as a promising process [7–9]. The membrane undergoes rotational motion to generate a shear force on forming droplets, acting tangential to the membrane surface. Additional detachment forces induced by rotation and milder fluid hydrodynamics serve as further optimisation towards producing more intricate microstructures.

At present, one of the limitations of membrane emulsification is the relatively low emulsion production rate as determined by the dispersed phase flux [10]. The flux largely depends on properties related to the membrane as well as the pressure applied and dispersed phase viscosity. However, some of these can be chosen by the operator and thus the process can be optimised depending on whether droplet size or throughput is the main priority [11]. Understanding of the interplay between processing and formulation parameters remains a topic of much deliberation within the literature. Furthermore, there is overall limited research available on rotating membrane emulsification despite its potential advantages. The aim of this study is to gain insight into how O/W emulsion droplet size and production rate are affected by the flow behaviour of the dispersed phase (flow through the membrane) and continuous phase (flow within the processing vessel). The discussion considers a wide range of phenomena relevant to emulsification using SPG membranes, focussing towards higher throughput processing in order to make the process more industrially viable. In addition, this study is designed to further current understanding of the droplet formation mechanisms involved within this process, which in turn should allow for the development of approaches to precisely formulate specific emulsion microstructures.

2. Materials and methods

2.1. Materials

Oil-in-water emulsions containing 10 vol% of dispersed phase were produced in all cases. The oil phase was either commercially available sunflower oil or silicone oil (Sigma Aldrich, United Kingdom) with density values shown in Table 1. The aqueous phase was passed through a reverse osmosis unit and then a milli-Q water system. The emulsions were stabilised by Tween 20 (polysorbate 20, Sigma Aldrich, United Kingdom) dissolved in the continuous phase using at a concentration of 1 wt% of the whole emulsion system. The continuous phase viscosity was modified using varying quantities of Glycerol (Sigma Aldrich, United Kingdom) between 1 and 87.5 wt%. All materials were used with no further purification or modification of their properties.

Table 1
Dispersed phase density values used to convert mass flow rates into dispersed phase fluxes.

Dispersed phase	Density (kg m^{-3})
Sunflower oil	919
Silicone oil (0.012 Pa s)	930
Silicone oil (0.023 Pa s)	950
Silicone oil (0.085 Pa s)	960

2.2. Experimental setup and procedure

The experiments were performed using a tubular, hydrophilic SPG membrane of 6.1 μm mean pore size (SPG Technology Co. Ltd., Miyazaki, Japan). The membrane dimensions were 10 mm outer diameter and 45 mm length, corresponding to an effective membrane surface area of 14.1 cm^2. The wall thickness of the membrane was approximately 1 mm. The membrane was mounted on an IKA Eurostar digital overhead stirrer and positioned in the processing vessel. This vessel was interchangeable allowing for different diameter vessels to be used. This altered the amount of continuous phase within the vessel since the membrane had to be submerged during process operation. Emulsion batch sizes between 20 and 360 g were produced. The membrane rotational speed in each experiment was kept constant between 100 and 2000 RPM. The transmembrane pressure was also held at a fixed value ranging from 0.1 to 1.8 bar (gauge). Since the outer vessel was open to atmosphere, the continuous phase was considered to be at atmospheric pressure throughout the whole fluid since the hydrostatic pressure exerted was negligible.

The schematic of the equipment setup is shown in Fig. 1. The oil phase was introduced to the inside of the membrane tube at the beginning of the experiment with the opening of the dispersed phase valve. Pressurisation of the dispersed phase storage tank with compressed air enabled the oil to permeate through the membrane to the outer continuous phase. Once the required mass of oil was added, the experiment was stopped by closing the dispersed phase valve and venting the storage tank.

2.3. Droplet size measurements

Droplet size distribution of all emulsion samples were measured using a Malvern Mastersizer (United Kingdom) with a hydro 2000 small volume sample dispersion unit. Droplet sizes given here was expressed as volume weighted mean diameter ($d_{4,3}$).

2.4. Interfacial tension measurements

Interfacial tension (IFT) values were measured using a goniometer Easydrop from Kruss (Germany). The pendant drop method was used to determine the interfacial tension at 20 °C between a droplet of dispersed (oil) phase formed from a 1.8 mm diameter needle within a cuvette containing the continuous (aqueous) phase. These measurements were taken over a period of 1800s at 30 s intervals to acquire both initial and equilibrium interfacial tension values. Due to the nature of the measurements, there is an inherent time delay (of 3.5 s) between the point when the two phases first encounter one another and the point at which the instrument starts measuring. As such, it is not possible to measure interfacial tension phenomena that occur over the extremely small timescales when the two phases are first introduced. In order to be able to obtain a relatively accurate estimate of interfacial tension values over these timescales, the follow approach was taken. Interfacial tension measurements were undertaken over a duration of 60 s at much shorter time intervals (≈ 0.2 s) in order to obtain a logarithmic function representing the
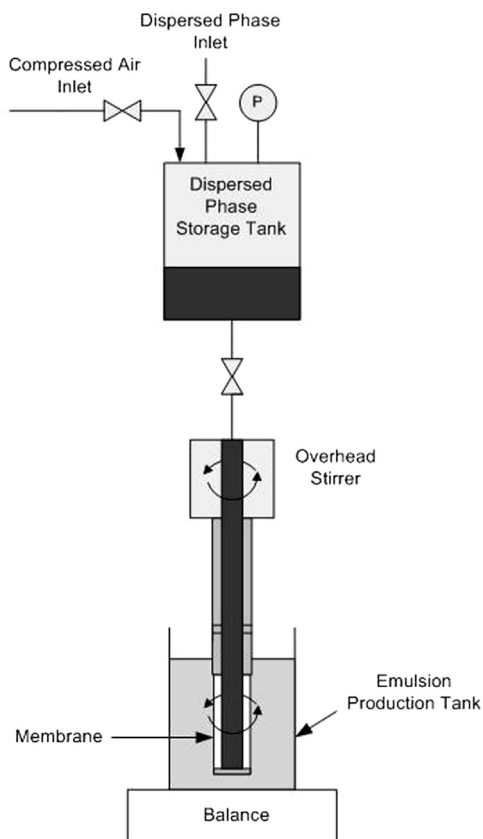
Fig. 1. Schematic diagram of the rotating membrane emulsification system used in this study.

rate of interfacial tension decrease. This process was repeated ten times to provide confidence in the rate behaviour of the systems investigated and to allow for approximation, through extrapolation, of the IFT values at times smaller than those experimentally achievable by the used instrumentation.

2.5. Viscosity measurements

The bulk viscosity was measured using a Bohlin Gemini HR Nano from Malvern Instruments (United Kingdom) with a concentric cylinder C25 DIN 53019 geometry at 20 °C. Viscosity measurements on both dispersed and continuous phases were performed by applying a range of shear rates between 0.1 and 995 s^{-1}.

2.6. Dispersed phase flux measurements

During emulsion production, the change in mass of the continuous phase vessel due to oil addition was recorded as a function of time. Therefore the dispersed phase flux values can be obtained using

$$J_d = \frac{M_d}{\rho_d A_m t_p}$$

(1)

where M_d is the mass of dispersed phase added, ρ_d is the disperse phase density, A_m is the membrane surface area and t_p is the processing time.

3. Results and discussion

3.1. Modification of dispersed phase flow behaviour

3.1.1. Effect of transmembrane pressure

Fig. 2 shows the resulting droplet size of the emulsion at different transmembrane pressures across a range of rotational speeds. The trend observed in general was that with increasing pressure, the droplet size decreased to a minimum before gradually increasing upon further pressure application. This behaviour is more prominent when the rotational speed, and hence the shear rate is low (i.e. 100 RPM). It is highly likely that to some extent coalescence is a contributing factor to the relatively large droplet sizes under these processing conditions, since these droplet sizes vary between 8.6 and 17.2 times larger than the pore diameter i.e. the upper end of the ratio values suggested by other authors [4,10]. Furthermore, droplet size distribution span values $(d_{90}-d_{10}/d_{50})$ across the whole data set range dramatically between 0.720 and 2.210 depending on processing conditions.

Within literature, the effect of transmembrane pressure (TMP) in membrane emulsification is contentious with the majority suggesting the droplet size increases with increasing transmembrane pressure [12–14]. Abrahamse et al. [15] found the droplet size to decrease with increasing transmembrane pressure. Within this study, it is observed that there is an initial decrease followed by an increase agreeing with the work of Vladisavljevic et al. [16]. It is therefore logical to suggest that there are multiple, contrasting factors affecting the droplet size produced. Droplet size increase with increasing pressure is attributed to higher interfacial tension values at small droplet formation times [13] and significant mass transfer via the droplet neck during detachment [14]. On the other hand, explanations for size decrease are that steric hindrance aids detachment of droplets from the membrane surface [15] and formation occurs from smaller diameter pore channels that were previously inactive at lower pressure [16]. The graph presented in Fig. 2 can be essentially divided into three regions with regards to TMP; a droplet decrease to a minimum (< 0.5 bar), a gradual increase in droplet size (0.5–1.5 bar) and then a rapid increase with polydisperse droplet sizes formed (> 1.5 bar). The exact transitional point between the regions depends on the rotational speed so approximations are stated to enable clarity during the discussion. Although not observed for the experimental conditions studied for systems shown in Fig. 2, in the later parts of the discussion and for systems of higher IFT values, the existence of a fourth region, in which a droplet size plateau is observed, will be proposed.
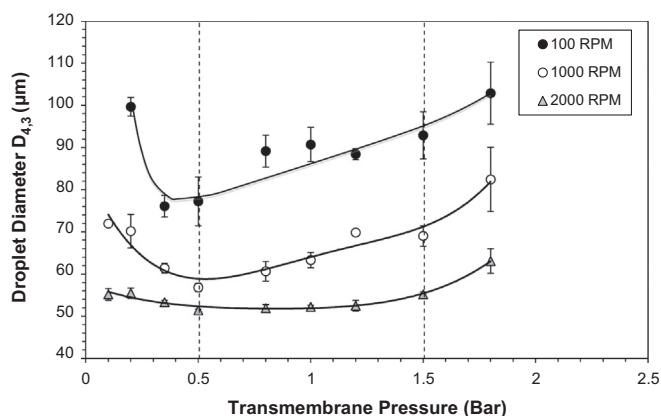

Fig. 2. The influence of transmembrane pressure on the mean droplet size for different rotational speeds. The emulsions are 10 vol% sunflower oil stabilised by 1 wt% Tween 20. The error bars represent one standard deviation of a triplicate of experimental runs.

At pressures < 0.5 bar the droplet size decreases with the extent depending on the rotational speed. At 100 RPM, this decrease is significant (22.5%, from 99.6 µm to 77.2 µm) whilst at 2000 RPM the decrease is almost negligible (6.9%, from 55.5 µm to 51.4 µm). The droplet size distribution span values follow a similar trend decreasing from 1.786 to 1.058 at 100 RPM whilst at 2000 RPM they decrease from 0.784 to 0.722. The observed decrease in droplet diameter with increasing rotational speeds are explained by the higher drag and centrifugal forces aiding earlier detachment with increasing rotational frequency. In the case of 0.1 bar TMP and 100 RPM, the emulsion phase separated completely. It is unlikely that such a dramatic destabilisation between 0.1 and 0.2 bar could be explained purely by the activation of smaller pores on the surface forming smaller droplets as postulated by Vladisavljevic et al. [16]. Furthermore, if steric hindrance to aid droplet detachment as suggested by Abrahamse et al. [15] is the explanation then surely a dramatic droplet size decrease would also be experienced (but without complete phase separation) at the higher rotational speeds. Therefore, it is proposed that droplet coalescence at the membrane surface would explain the trends. With an increase in TMP, the droplet formation time will decrease and thus droplets spend less time at the membrane surface i.e. where there is a higher risk for droplet coalescence [17]. Furthermore, the magnitude of the linear momentum and dynamic effect of pressure forces will increase aiding both detachment and displacement away from the membrane surface. If droplets remain nearby to the membrane surface and are not swept away into the bulk continuous phase, coalescence events between them and forming droplet (at the membrane surface) would not be inconceivable leading to formation of a more polydisperse emulsion (i.e. greater droplet size distribution span values). Coalescence would be promoted when an increase in active pore fraction leads to droplets forming more closely together. However the distance between active pores across the membrane surface is over 100 µm (number of pores from [18] assuming a triangular tessellation of evenly distributed pores) meaning contact even at higher pressures is unlikely. It appears longer droplet formation times implicit to low shear rates and low pressures pose a higher risk in terms of coalescence occurring, and hence production of larger droplet sizes and even phase separation can occur.

As the pressure is increased between 0.5 and 1.5 bar, the extent of droplet size increases gradually but dependency on the rotational speed is still observed. At 100 RPM, an increase of 20.3% (up to 92.9 µm) is observed whilst at 2000 RPM the increase is 7.3% (up to 55.2 µm). It is hypothesised that the effect of coalescence is now minimised (since droplets spend less time at the membrane surface) and as such, the droplet size is determined by the dispersed phase mass transfer rate as the droplet detaches from the membrane surface and thus on the TMP. This theory was discussed within the work of Peng and Williams [14] in which the final droplet size was suggested to consist of volumetric contributions from both the growth and detachment stages. The growth volume depended on the size needed for the detachment forces to overcome the interfacial tension force. However, the detachment volume scaled linearly with dispersed phase flux with a greater contribution towards the final volume if the flux was high or the detachment time was long. This is shown by

$$V_f = V_g + V_d = V_g + Q_D t_d \tag{2}$$

where V_g is the volume of the droplet at the end of the growth stage, V_d is the volumetric contribution from the detachment stage, Q_D is the volumetric flow rate through a single pore channel and t_d is the droplet detachment time [14]. At a low rotational speed, the droplet detachment time is likely to be longer compared to higher speeds (since lower magnitude of force to displace droplets from the membrane surface) and as such the mass transfer of dispersed phase during detachment is more significant. With high rotational speeds, the droplet detachment time approaches close to zero meaning any variation in volumetric flow rate (determined by TMP) does not significantly influence the volumetric contribution during detachment. The final droplet volume is likely to coincide with the growth volume which will be smaller due to dominating drag and centrifugal detachment forces compared to at low speed.

Finally, at pressures > 1.5 bar the droplet size begins to increase rapidly and erratically (as shown by the large error bars). Evaluation of the Capillary number reveals there is a likely change in the droplet formation mechanism from dripping to jetting. The Capillary number is defined by

$$Ca_d = \frac{\mu_d \overline{v_d}}{\gamma} \tag{3}$$

where μ_d is the dispersed phase viscosity, $\overline{v_d}$ is the average dispersed phase velocity in the pore channel (estimated using
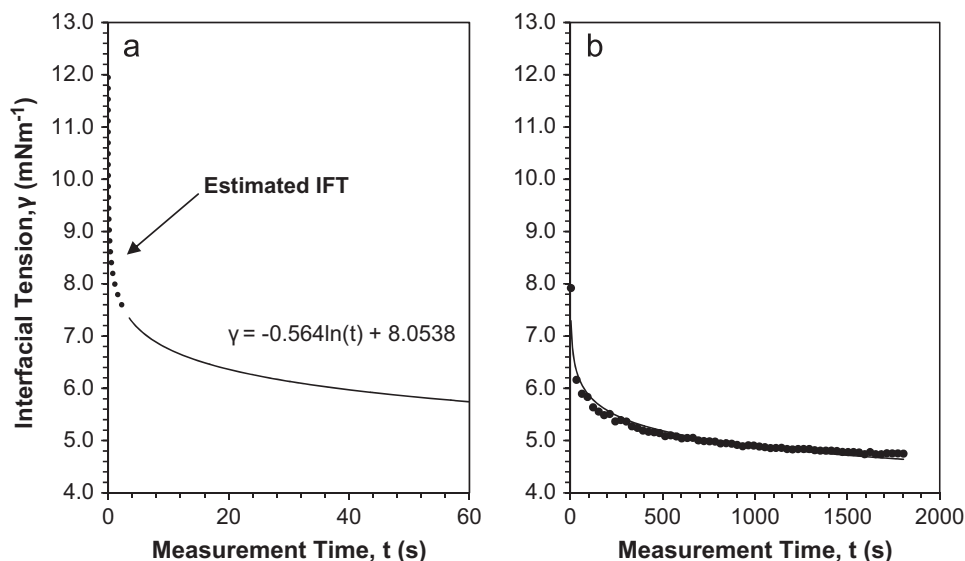
Fig. 3. Dynamic interfacial tension between sunflower oil and 1 wt% Tween 20 solution. (a) shows the initial decrease whilst (b) shows the system equilibrium value. Note: dotted line and solid line represent back-calculated and measured interfacial tension values respectively.

the Fanning equation for laminar flow in a tubular pipe) and γ is the interfacial tension. The interfacial tension value for 1 wt% Tween 20 and sunflower oil is shown in Fig. 3. The complete line represents almost continuous measurement of the interfacial tension whilst the dotted line is back-calculated from the dynamic rate since there was a 3.5 s delay between formation and measurement. Droplet formation and detachment typically occurs within a couple of seconds [15] so using the equilibrium interfacial tension value would be a significant underestimation [19]. For example, the interfacial tension varies between 10.7 m Nm^{-1} at 0.01 s and 7.7 m Nm^{-1} at 2 s (Fig. 3a) – values much higher than the equilibrium value of 4.8 m Nm^{-1} (Fig. 3b).

At pressures beyond 1.5 bar, the dispersed phase velocity exceeds 0.0023 ms^{-1} so evaluating for the Capillary number with sunflower oil of viscosity 0.066 Pa s equates to values greater than 0.014. Thus, the Capillary number is tending towards the approximate threshold of 0.056 suggested by Sugiura et al. as the jetting point [20]. At low droplet formation times that are achieved with high pressure or high rotational speed, detachment will occur in a period of higher interfacial tension which minimises the Capillary number slightly. However, the velocity increase induced by higher pressure is far more influential compared to any slight differences in the interfacial tension. Using this logic, this would explain why the droplet size increases more erratically at 100 RPM compared to 2000 RPM as lower drag and centrifugal forces allow sufficient time for the interfacial tension value to tend more towards the equilibrium value (increasing Capillary number).

What is clear is that the transmembrane pressure has differing effects on the droplet size depending on the amount of shear applied. Both a decrease following by an increase in droplet size, as well as an almost single increase has been demonstrated within this study across the range of the pressures investigated. This may possibly explain the variation in observations for this parameter within the literature.

The dispersed phase flux through the membrane is presented in Fig. 4a. Knowledge of the flux is important to correlate the transmembrane pressure to the demonstrated permeability of the membrane. As expected, with increasing pressure the dispersed phase flux also increases as determined by Darcy's law. Typical values of 100–200 L m^{-2} h^{-1} are achieved at 0.2 bar compared to 2000–2600 L m^{-2} h^{-1} at 1.5 bar. This relationship shows an exponential increase in flux due to increased pore activation of the SPG membrane when greater pressure is applied. Vladisavljevic

et al. [16] found the flux of water was proportional to the transmembrane pressure to the power of a value between 2.3 and 2.7 when using SPG membranes. However, a value of 1.28 is demonstrated within this work which is likely to be because the dispersed phase used is of higher viscosity and has different wetting properties within the membrane structure. In all cases, the percentage of pores active remained between 0.9% and 2.7% (Fig. 4b) which is similar to values quoted in previous literature [16,21]. The active pore fraction was calculated by firstly evaluating the demonstrated permeability (K) of the SPG membrane at a given TMP (ΔP_{tm}); combining Darcy's law with Eq. (1):

$$J_d = \frac{K\Delta P_{tm}}{\mu_d L_p} = \frac{M_d}{\rho_d A_m t_p}$$

$$K = \frac{\mu_d L_p M_d}{\Delta P_{tm}\rho_d A_m t_p} \quad (4)$$

where K is the membrane permeability, ΔP_{tm} is the applied transmembrane pressure and L_p is the pore channel length (estimated as the membrane thickness multiplied by a tortuosity factor of 1.28 for SPG membranes [18]). Using this value within an expression of permeability given by O'Brien et al. [22] allows for the active pore fraction (α) to be estimated:

$$K = \alpha d_p^2 \phi^{1.5}$$

$$\alpha = \frac{K}{d_p^2 \phi^{1.5}} \quad (5)$$

where α is the active pore fraction, d_p is the membrane pore diameter and ϕ is the membrane porosity which is approximately 0.56 [18]. It is likely that the flux may be slightly hindered by the rotational motion of the membrane (acting perpendicular to the flow at an instantaneous point in time) as the disperse phase is forced against one side of the pore channel as it traverses the membrane structure increasing frictional losses. If this is the case, it is likely the active pore fraction will be slightly higher than calculated.

3.1.2. Effect of dispersed phase viscosity

The dispersed phase viscosity has an influence on the measured droplet size as observed in Fig. 5. With increasing pressure, the droplet size decreased to a minimum with the extent depending on the viscosity. For the lowest viscosity silicone oil (0.012 Pa s),
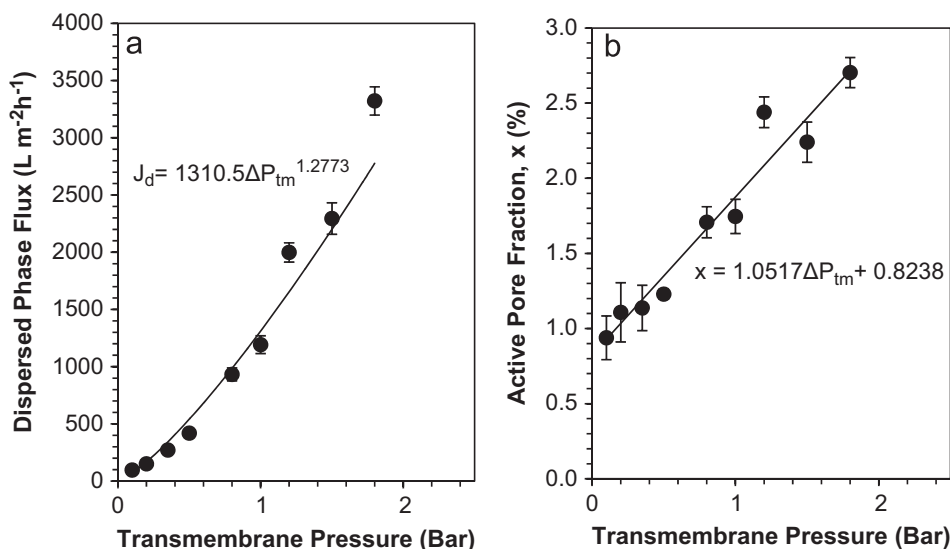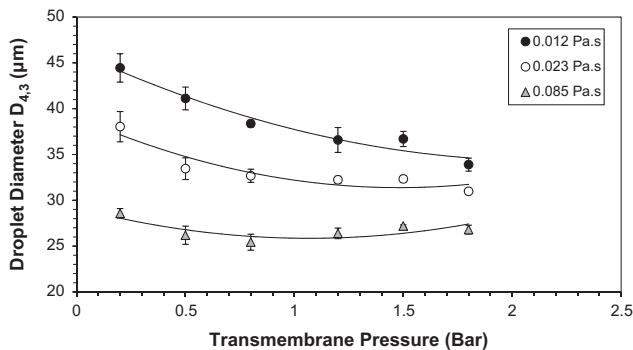

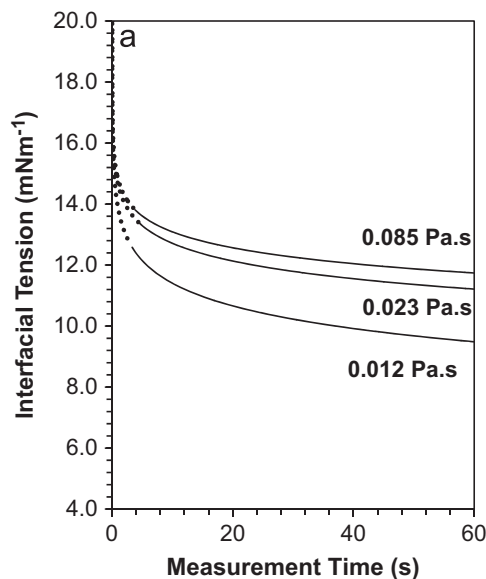**Fig. 4.** Influence of transmembrane pressure on the dispersed phase flux (a) and active pore fraction (b) for a 6.1 μm pore diameter, hydrophilic SPG membrane.

the decrease between 0.2 and 1.8 bar was 23.8% (from 44.5 μm to 33.9 μm) whereas for the highest viscosity oil (0.085 Pa s), the decrease was 6.3% (from 28.6 μm to 26.8 μm). Generally, the droplet sizes were the largest for the 0.012 Pa s oil perhaps because the lower resistance to flow enables greater mass transfer during the detachment stage. Furthermore, it was suggested that the drag coefficient adopted (typically 1.7 for a rigid sphere [23]) was a possible variable within force balance models [24]. It is proposed that a higher viscosity dispersed phase droplet potentially resembles a rigid sphere more closely than a lower viscosity equivalent and therefore experiences greater drag to aid detachment. The density differences between the silicone oils also alter the point of detachment with heavier droplets experiencing more centrifugal force at the expense of the less significant buoyancy force. Upon detachment, a droplet of more dense material is likely to be displaced further towards the outer vessel wall and away from the pore opening, hence limiting any potential coalescence. This is comparable to a centrifuge in which heavier material moves to the outer edges during rotation.

In contrast with Fig. 2, only two distinct regions are observed; an initial droplet size decrease that may possibly be attributed to coalescence, followed by a plateau in the size. The latter region was typically observed within microchannel emulsification and is known as the 'size-stable zone' [25,26]. The prominence of this region depends on high interfacial tension values which cause non-spherical, deformed droplets to transform back to spheres by
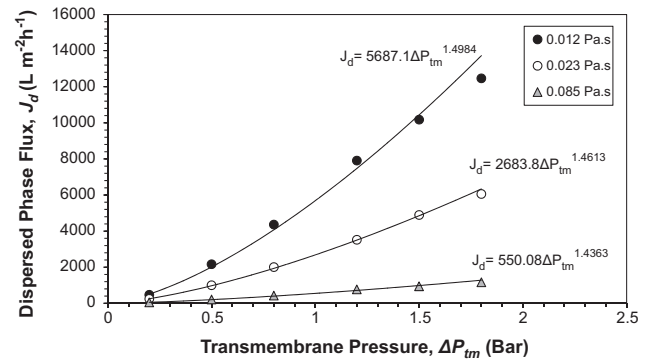
Fig. 7. Influence of transmembrane pressure on the dispersed phase flux for differing viscosity silicone oil through a 6.1 μm pore diameter, hydrophilic SPG membrane.
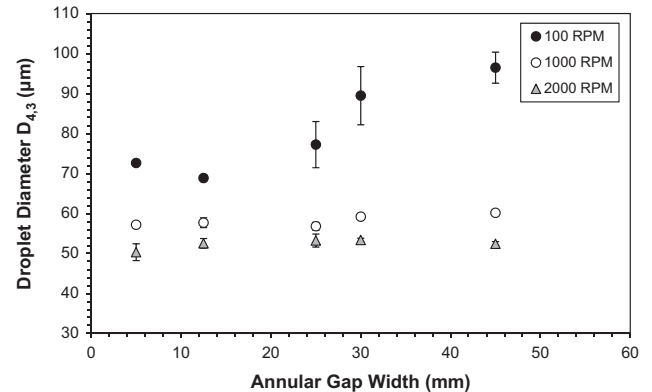

Fig. 5. The influence of transmembrane pressure on the mean droplet size for different oil viscosities. The emulsions are 10 vol% silicone oil stabilised by 1 wt% Tween 20. The error bars represent one standard deviation of a triplicate of experimental runs.

Fig. 8. The influence of gap width and rotational speed on the mean emulsion droplet size at 0.5 bar. The emulsions are 10 vol% sunflower oil stabilised by 1 wt% Tween 20. The error bars represent one standard deviation and where not visible are smaller than the symbols.
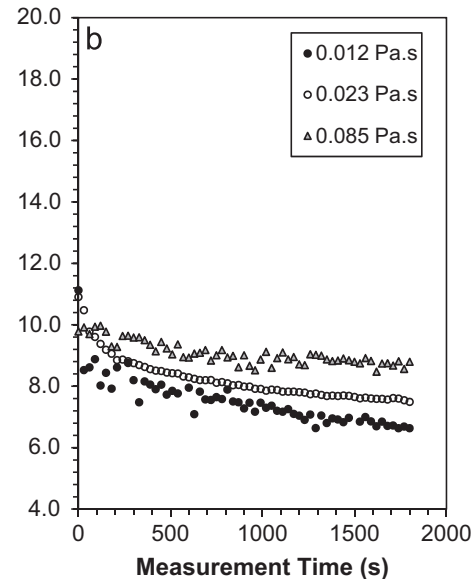
Fig. 6. Dynamic interfacial tension between silicone oil of varying viscosity and 1% Tween 20 solution. (a) shows the initial decrease whilst (b) shows the system equilibrium value. Note: dotted line and solid line represent back-calculated and measured interfacial tension values respectively.

detaching in a bid to minimise their interfacial free energy – known as 'spontaneous transformation-based droplet formation'. As can be seen in Fig. 6, the interfacial tension between silicone oil and 1% Tween 20 solution is higher than for sunflower oil since there are no triglyceride impurities and hence the 'size-stable zone' is not apparent in Fig. 2. A more viscous silicone oil also has a higher interfacial tension value due to high molecular weight siloxane chains having greater Van der Waals' forces between them and hence a greater cohesive energy. Upon further pressure increase (beyond the 1.8 bar maximum TMP studied here), it is predicted the droplet size will begin to increase as the volumetric contribution during detachment becomes significant and eventually droplet production through a jetting mechanism will occur. However, these latter two regions (unlike in Fig. 2) are not observed here. Despite the high dispersed phase velocity achievable with 0.012 Pa s silicone oil (0.0015–0.014 ms^{-1} across the pressure range), the high interfacial tension during detachment (between 18.8 m Nm^{-1} at 0.01 s and 13.1 m Nm^{-1} at 2 s) ensures the Capillary number does not exceed 0.010.

The dispersed phase flux for the respective silicone oils is presented in Fig. 7. As expected, higher flux values are achieved with the lower viscosity dispersed phase since there is less resistance to flow. In this case, flux values between 470 and 12,500 L m^{-2}h^{-1} were measured for the 0.012 Pa s silicone oil compared to 50–1200 L m^{-2}h^{-1} for the 0.085 Pa s oil. The exponential power number ranges between 1.43 and 1.49 with increasing viscosity; the 0.012 Pa s silicone oil has the lowest surface tension allowing it to permeate more readily through the tortuous pore channels previously inactive at lower pressure.

3.2. Modification of continuous phase flow behaviour

3.2.1. Effect of annular gap width

As shown in Fig. 8 (TMP=0.5 bar), the annular gap width between the membrane surface and the outer vessel wall influences the droplet size. If the gap is narrow or the rotational speed is high, a greater shear rate is generated which should lead to smaller droplets being formed. Therefore, the data can be re-plotted as a function of shear rate at the membrane surface as shown in Fig. 9 using

$$\dot{\gamma} = \frac{\pi r_1^2 n_1}{15(r_2^2 - r_1^2)} \qquad (6)$$

where $\dot{\gamma}$ is the shear rate, r_1 and r_2 are the radii of the cylindrical membrane and emulsion production vessel respectively and n_1 is the membrane rotational speed [8]. However, the flow regime of the continuous phase must also be considered. With a wider gap between the membrane and the outer vessel wall, both the Reynolds (Eq. (7)) and Taylor (Eq. (8)) numbers will be higher which can lead to turbulent flow and the development of Taylor
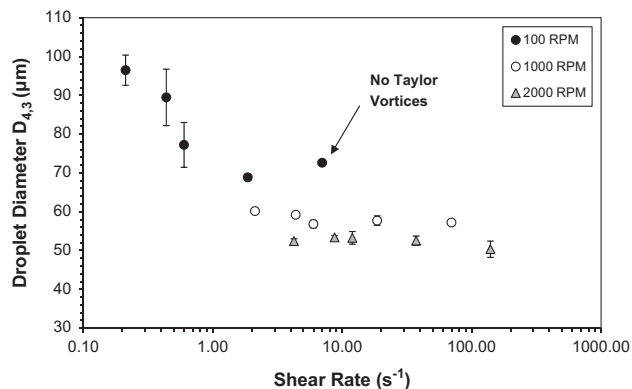

Fig. 9. Relationship between droplet size and the shear rate at the membrane surface for the different gap widths and rotational speeds investigated, at 0.5 bar.
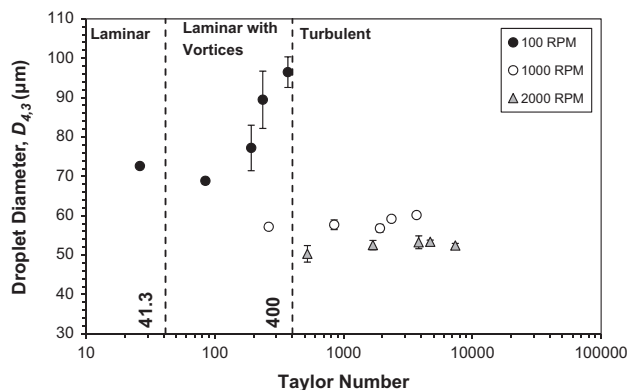

Fig. 10. Relationship between mean emulsion droplet size and (continuous phase) Taylor number as a function of rotational speed, at a transmembrane pressure of 0.5 bar.

Table 2
Calculated values characterising the continuous phase flow behaviour for the respective configurations investigated using a 1% wt. Tween 20 solution.

Gap size (mm)	Rotational speed (RPM)	Droplet diameter $D_{4,3}$ (μm)	Shear rate (s^{-1})	Reynolds number	Taylor number
5	100	72.6	6.98	32	26
12.5	100	68.9	1.86	80	84
25	100	77.2	0.60	160	191
30	100	89.5	0.44	192	235
45	100	96.5	0.21	288	369
5	1000	57.2	69.8	320	261
12.5	1000	57.7	18.6	800	844
25	1000	56.8	5.98	1601	1914
30	1000	59.2	4.36	1921	2353
45	1000	60.2	2.12	2882	3686
5	2000	50.3	139.6	640	523
12.5	2000	52.6	37.2	1601	1688
25	2000	53.3	12.0	3202	3827
30	2000	53.4	8.73	3842	4706
45	2000	52.4	4.23	5764	7373

vortices [27].

$$Re_c = \omega_1 r_1 (r_2 - r_1) \frac{\rho_c}{\mu_c} \qquad (7)$$

$$Ta = Re_c \sqrt{\frac{2(r_2 - r_1)}{r_1 + r_2}} \qquad (8)$$

where Re_c and Ta are the Reynolds number and Taylor number for the continuous phase respectively, ω_1 is the angular velocity of the membrane surface, ρ_c is the density and μ_c is the viscosity of the continuous phase. The values that define the continuous phase flow behaviour are presented in Table 2, where a 1 wt% Tween 20 solution was measured to have a viscosity of 0.0013 Pa s and a density of 999.0 kg m^{-3}.

With a rotational speed of 100 RPM, the shear rate at the membrane surface varied across a range of 0.21–6.98 s^{-1}. Increasing the gap size between 12.5 and 45 mm, the droplet size increased almost linearly from 68.9 μm to 96.5 μm. This is attributed to low shear rates indicating droplets grow much larger before experiencing sufficient drag force that induces detachment. With a wider outer vessel, the velocity gradient of the continuous phase in the radial direction is reduced. Therefore, droplets need to protrude further to encounter a significant velocity difference between the membrane surface and the continuous phase. Coalescence may also be a factor at the lowest shear rates as the probability of droplet–droplet interactions on the membrane surface increases with larger droplets. Within this range of gap sizes, vortices are produced as the Taylor number exceeds the critical value of 41.3 as shown in Fig. 10. However in the case of the 5 mm gap, vortices are not present since the Taylor number for the system is 26. Thus, a larger than expected droplet size of 72.6 μm is obtained despite the higher shear rate as seen in Fig. 9. This is consistent with the findings by Schadler and Windhab [27].

Increasing the membrane rotational speed to an intermediate level of 1000 RPM, this broadened the shear rate range experienced by droplets at the membrane surface between 2.12 and 69.8 s^{-1}. The droplet size remained relatively constant (56.8–60.2 μm) regardless of the shear rate applied. This suggests that with the rotating membrane system, as with previous findings with the cross-flow system, the droplet size tends to a value that is independent of the shear rate applied. However, droplet sizes produced at 1000 RPM were smaller than those produced at 100 RPM because of higher shear rates alongside the presence of Taylor vortices. The flow regime of the continuous phase in all cases apart from with a 5 mm gap was turbulent although there is no noticeable difference in droplet size either side of the threshold Taylor number of 400.

At 2000 RPM, shear rates of 4.2–139.6 s^{-1} were generated across the range of gap widths investigated and turbulent flow was present in all cases (Ta > 400). Droplets were consistently 50.3–53.4 μm in diameter suggesting the size was again independent of the shear rate applied. In some cases, the droplet size was smaller than when the system was operated at a higher shear rate. For example, using a 45 mm gap at 2000 RPM corresponded to a shear rate of 4.23 s^{-1} and formed droplets of diameter 52.4 μm. However, a 12.5 mm gap at 1000 RPM induced a shear rate of 18.6 s^{-1} and produced droplets of diameter 57.7 μm. As previously discussed, this is the result of centrifugal force effects and therefore implies that in the region where droplet size is independent of the applied shear rate, generating a higher centrifugal force can further modify the size.

3.2.2. Effect of continuous phase viscosity

The viscosity of the continuous phase has previously been shown to affect the droplet size with a rotating membrane configuration [7,28]. In these studies, the droplet size decreased when using a more viscous continuous phase since the drag force increases in a directly proportional manner. It was therefore expected that investigation of this parameter by thickening the continuous phase with 1–50 wt% of glycerol would provide a similar trend. Glycerol was selected since it demonstrates Newtonian behaviour across the range of shear rates investigated here (0.60–104.7 s^{-1}) allowing a constant viscosity value as the rotational speed and gap size is altered to modify the shear rate. The properties of the solutions are presented in Table 3. As can be seen in Fig. 11 (TMP=0.5 bar), surprisingly the smallest droplet sizes (37.1–73.6 μm) were achieved with the lowest viscosity continuous phase of 1 wt% glycerol compared to 25 wt% glycerol (450–155.4 μm). This is despite the interfacial tension retaining the droplet at the membrane surface being slightly higher, since glycerol acts as a co-emulsifier [29]. Furthermore, differentiating the power curve functions shows the droplet size decreases much more rapidly with increasing shear rate for higher viscosity systems up until 25–50 wt% glycerol where the curves are parallel.

These observations may perhaps be explained by considering the movement of droplets within the continuous phase. With a more viscous continuous phase, droplets cannot easily move away from the membrane surface towards the outer edge of the emulsification vessel since their movement is hindered by viscosity and density effects. As a consequence, detached droplets remain within the vicinity of forming droplets increasing the likelihood of coalescence. This would explain why complete phase separation is observed in the case of 50wt % glycerol under a shear rate of 0.60 s^{-1}. Also, very viscous solutions are more laminar within a concentric cylinder setup and as such may not develop Taylor vortices to sweep droplets away. This can be seen in the case of 50% glycerol and an applied shear rate of 52.4 s^{-1} (which corresponds to 750 RPM and a 5 mm gap size). Under these conditions, the Taylor number is 31 and hence the droplet size is much larger than expected (126.6 μm). Overall, the droplet size decrease is rapid for more viscous solutions upon increasing the shear rate. As coalescence effects are negated, the higher drag

Table 3

Physical properties of solutions investigated when modifying continuous phase viscosity with glycerol.

Ratio of glycerol: water (wt%)	Equilibrium IFT w/SFO & 1% Tween 20 (m Nm^{-1})	Viscosity w/1% Tween 20 (Pa s)	Density w/1% Tween 20 (kg m^{-3})
1:99	4.7	0.00186	1001.6
10:90	4.1	0.00226	1025.0
25:75	3.5	0.00332	1063.9
50:50	2.4	0.00916	1128.7
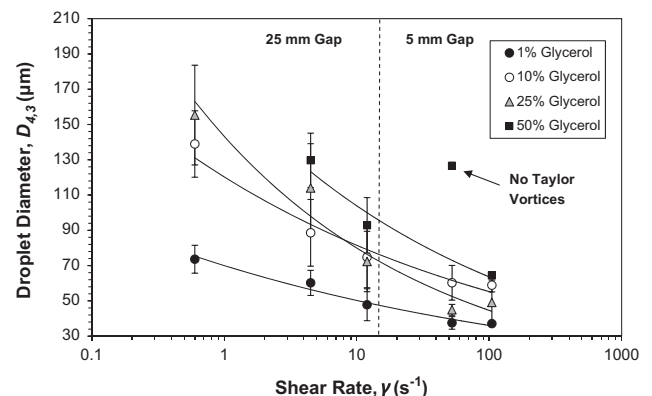
Fig. 11. The influence of continuous phase viscosity and shear rate on the mean droplet size at 0.5 bar using a 6.1 μm pore diameter, hydrophilic SPG membrane.

force allows droplets to detach much earlier from the membrane surface. It is therefore predicted that further shear rate modification $\geqslant 104.7\ \mathrm{s}^{-1}$ that droplet sizes will be smaller for higher viscosity continuous phase systems.

4. Conclusions

The effect of transmembrane pressure, shear rate, dispersed and continuous phase viscosity on the final droplet size and flux has been investigated for a rotating membrane emulsification system. O/W emulsion droplets of average diameter 23.4–216.6 µm have been produced using an SPG membrane of 6.1 µm pore diameter. In this article, a number of complex processing effects have been discussed through consideration of the fluid flow and interfacial behaviour of the two phases.

Considering the dispersed phase flow behaviour effects on droplet size, four distinct regions can be seen across the range of transmembrane pressures investigated. Firstly, a decrease in size across low pressures (at approximately < 0.5 bar) which is attributed to coalescence at the membrane surface during long droplet formation times. Secondly, a plateau in size known as the 'size-stable' zone which occurs due to the spontaneous transformation-based droplet formation mechanism in systems with high interfacial tension (i.e. with silicone oils). Thirdly, an eventual increase in droplet size as significant mass is transferred via the droplet neck during detachment. The volumetric contribution during this stage depends primarily on the droplet detachment time at the dispersed phase flux and thus can become negligible at increased rotational speeds (> 1000 RPM). This is due to higher drag and centrifugal forces to ensure earlier detachment and displace droplets quickly away from the membrane surface. It is also suggested that viscous dispersed phase droplets may experience a higher drag coefficient since they resemble more rigid spheres; an assumption within drag force calculations. Finally, if the interfacial tension is low and dispersed phase flux (or more specifically the pore fluid velocity) is sufficiently high, jetting of the dispersed phase may occur (approximately > 1.5 bar). In this case, the Capillary number defining this flow behaviour approaches the threshold value of 0.056 that is previously suggested in literature.

The flux through the membrane increases with high pressure and low dispersed phase viscosity as defined by Darcy's law. Values between 50 and 12,500 L m^{-2} h^{-1} were measured for oil viscosities between 0.012 and 0.085 Pa s across applied transmembrane pressures between 0.1 and 1.8 bar. For SPG membranes, this relationship between flux and pressure is exponential rather than directly proportional since membranes demonstrate a variable permeability. The percentage activation of tortuous pore channels depends on the applied transmembrane pressure. The calculated values for active pore fraction ranged between 0.5% and 2.7% coinciding with previous findings for SPG membranes.

The continuous phase flow behaviour also determines the droplet size produced primarily by altering the drag force acting on the droplet. By increasing the shear rate (through higher rotational speeds and narrower annular gap widths), the droplet size tends to a minimum independent of the applied shear as commonly observed within cross-flow membrane emulsification. However, the rotational speed contributes an additional centrifugal force to enable even earlier detachment from the membrane surface and thus further reducing the droplet size. Another key consideration is where Taylor vortices can form and in their absence below a critical Taylor number of 41.3, droplet sizes are significantly larger. This is possible particularly for low speed, narrow gap or high viscosity continuous phase systems. Finally, if there is a significant density difference between the two phases

(dispersed phase being typically lower for O/W systems) or if the aqueous continuous phase viscosity is high, there is a potential for droplets to not be displaced sufficiently away from the membrane surface but remain within the vicinity of other forming droplets. This is likely to increase coalescence phenomena, which is generally unfavourable during emulsification processing.

Nomenclature

A_m	Membrane surface area [m^2]
Ca_d	Capillary number for dispersed phase [dimensionless]
d_p	Membrane pore diameter [m]
J_d	Dispersed phase flux [m^3 m^{-2} s^{-1}]
K	Permeability [m^2]
L_p	Pore channel length [m]
M_d	Mass of dispersed phase added [kg]
n_1	Membrane rotational speed [Rotations per minute; RPM]
Q_D	Volumetric flow rate through a pore channel [m^3 s^{-1}]
r_1	Membrane radius [m]
r_2	Emulsification vessel radius [m]
Re_c	Reynolds number for continuous phase [dimensionless]
Ta	Taylor number for continuous phase [dimensionless]
t_d	Droplet detachment time [s]
t_p	Processing time for emulsification [s]
$\overline{v_\mathrm{d}}$	Average velocity of dispersed phase within pore channel [ms^{-1}]
V_d	Volumetric contribution towards final droplet size during detachment stage [m^3]
V_f	Final droplet volume [m^3]
V_g	Volume of droplet at end of growth stage [m^3]

Greek letters

α	Membrane active pore fraction [dimensionless]
$\dot{\gamma}$	Shear rate at the membrane surface [s^{-1}]
γ	Interfacial tension between oil/water system [Nm^{-1}]
ΔP_tm	Transmembrane pressure [Pa]
μ_c	Viscosity of continuous phase [Pa s]
μ_d	Viscosity of dispersed phase [Pa s]
ρ_c	Density of continuous phase [kg m^{-3}]
ρ_d	Density of dispersed phase [kg m^{-3}]
φ	Membrane porosity [dimensionless]
ω_1	Angular velocity of membrane surface [Rotations per second]

References

[1] E.L. Paul, V.A. Atiemo-Obeng, S.M. Kresta, Handbook of Industrial Mixing: Science and Practice, vol. 1, John Wiley and Sons. Inc, Hoboken, New Jersey (2004) 1–1377.

[2] T. Nakashima, M. Shimizu, M. Kukizaki, Membrane emulsification by microporous glass, Key Eng. Mater. 61–62 (1991) 513–516.

[3] A.J. Gijsbertsen-Abrahamse, A. van der Padt, R.M. Boom, Status of cross-flow membrane emulsification and outlook for industrial application, J. Membr. Sci. 230 (1-2) (2004) 149–159.

[4] C. Charcosset, Preparation of emulsions and particles by membrane emulsification for the food processing industry, J. Food Eng. 92 (3) (2009) 241–249.

[5] H. Schubert, Advances in the mechanical production of food emulsions, in: Proceedings of the 7th International Congress on Engineering and Food, Part 1, 1997, pp. 82–87.

[6] F. Spyropoulos, R.D. Hancocks, I.T. Norton, Food-grade emulsions prepared by membrane emulsification techniques, Proc. Food Sci. 1 (2011) 920–926.

[7] N. Aryanti, R. Hou, R.A. Williams, Performance of a rotating membrane emulsifier for production of coarse droplets, J. Membr. Sci. 326 (1) (2009) 9–18.

[8] G.T. Vladisavljevic, R.A. Williams, Manufacture of large uniform droplets using rotating membrane emulsification, J. Colloid Interface Sci. 299 (1) (2006) 396–402.

[9] Q. Yuan, N. Aryanti, R. Hou, R.A. Williams, Performance of slotted pores in particle manufacture using rotating membrane emulsification, Particuology 7 (2) (2009) 114–120.

[10] S.M. Joscelyne, G. Tragardh, Membrane emulsification – a literature review, J. Membr. Sci. 169 (1) (2000) 107–117.

[11] F. Spyropoulos, D.M. Lloyd, R.D. Hancocks, A.K. Pawlik, Advances in membrane emulsification. Part B: recent developments in modelling and scale-up approaches, J. Sci. Food Agric. (2013) ⟨http://onlinelibrary.wiley.com/doi/10.1002/jsfa.6443/pdf⟩.

[12] R. Katoh, A. Furuya, K. Sotoyama, M. Tomita, Preparation of food emulsions using a membrane emulsification system, J. Membr. Sci. 113 (1) (1996) 131–135.

[13] V. Schroder, O. Behrend, H. Schubert, Effect of dynamic interfacial tension on the emulsification process using microporous, ceramic membranes, J. Colloid Interface Sci. 202 (2) (1998) 334–340.

[14] S.J. Peng, R.A. Williams, Controlled production of emulsions using crossflow membrane Part I: droplet Formation from a single pore, Chem. Eng. Res. Des. 76 (8) (1998) 894–901.

[15] A.J. Abrahamse, R. van Lierop, R.G.M. van der Sman, A. van der Padt, R.M. Boom, Analysis of droplet formation and interactions during cross-flow membrane emulsification, J. Membr. Sci. 204 (1–2) (2002) 125–137.

[16] G.T. Vladisavljevic, U. Lambrich, M. Nakajima, H. Schubert, Production of O/W emulsions using SPG membranes, ceramic α-aluminium oxide membranes, microfluidizer and a silicon microchannel plate – a comparative study, Colloids Surf. A: Physicochem. Eng. Asp. 232 (2–3) (2004) 199–207.

[17] E. Lepercq-Bost, M. Giorgi, A. Lsambert, C. Arnaud, Estimating the risk of coalescence in membrane emulsification, J. Membr. Sci. 357 (1–2) (2010) 36–46.

[18] G.T. Vladisavljevic, M. Shimizu, T. Nakashima, Permeability of hydrophilic and hydrophobic Shirasu-porous-glass (SPG) membranes to pure liquids and its microstructure, J. Membr. Sci. 250 (2005) 69–77.

[19] G. De Luca, A. Sindona, L. Giorno, E. Drioli, Quantitative analysis of coupling effects in cross-flow membrane emulsification, J. Membr. Sci. 229 (1–2) (2004) 199–209.

[20] S. Sugiura, M. Nakajima, N. Kumazawa, S. Iwamoto, M. Seki, Characterization of spontaneous transformation-based droplet formation during microchannel emulsification, J. Phys. Chem. B 106 (36) (2002) 9405–9409.

[21] G.T. Vladisavljevic, H. Schubert, Preparation and analysis of oil-in-water emulsions with a narrow droplet size distribution using Shirasu-porous-glass (SPG) membranes, Desalination 144 (1-3) (2002) 167–172.

[22] F.J. O'Brien, B.A. Harley, I.V. Yannas, L.J. Gibson, The effect of pore size on permeability and cell attachment in collagen scaffolds for tissue engineering, Technol. Health Care 15 (1) (2007) 3–17.

[23] M.E. O'Neil, A slow motion of viscous liquids caused by a slowly moving solid sphere, Chem. Eng. Sci. 23 (1964) 67–74.

[24] A. Timgren, G. Tragardh, C. Tragardh, Application of the PIV technique to measurements around and inside a forming drop in a liquid–liquid system, Exp. Fluids 44 (2008) 565–575.

[25] M. Kukizaki, Shirasu porous glass (SPG) membrane emulsification in the absence of shear flow at the membrane surface: influence of surfactant type and concentration, viscosities of dispersed and continuous phases, and transmembrane pressure, J. Membr. Sci. 327 (2009) 234–243.

[26] I. Kobayashi, M. Nakajima, S. Mukutaka, Preparation characteristics of oil-in-water emulsions using differently charged surfactants in straight-through microchannel emulsification, Colloids Surf. A: Physicochem. Eng. Asp. 229 (1–3) (2003) 33–41.

[27] V. Schadler, E.J. Windhab, Continuous membrane emulsification by using a membrane system with controlled pore distance, Desalination 189 (2006) 130–135.

[28] A.K. Pawlik, I.T. Norton, SPG rotating membrane technique for production of food grade emulsions, J. Food Eng. 114 (2013) 530–537.

[29] G. Yilmaz, R.O.J. Jongboom, J.J.G. van Soest, H. Feil, Effect of glycerol on the morphology of starch-sunflower oil composites, Carbohydr. Polym. 38 (1) (1999) 33–39.